HYDROLOGICAL PROCESSES
Hydrol. Process. **25**, 217–233 (2011)
Published online 1 September 2010 in Wiley Online Library
(wileyonlinelibrary.com) DOI: 10.1002/hyp.7838

Geostatistics for assessing the efficiency of a distributed physically-based water quality model: application to nitrate in the Seine River

Edwige Polus,* Nicolas Flipo, Chantal de Fouquet and Michel Poulin
MINES ParisTech, Centre de Geosciences, 35 rue Saint-Honoré, F-77305 Fontainebleau, France

Abstract:

This article shows how geostatistics can be used to reduce distributed physically based model (DPBM) uncertainties when assessing nitrate concentrations along a 250-km stretch of the Seine River. First of all, co-kriging is used to build a set of boundary conditions (BCs) (inlet concentrations from major tributary rivers) consistent with validation data. It partially addresses the issues of errors in data used as model input and errors in data to be compared with model outputs. Then the analysis of temporal variograms (simple variograms of observed and simulated concentrations, and their cross-variogram) reveals a clear mismatch between simulated and observed values that was not detected by classical objective functions [root mean squared error (RMSE), etc.]. Variograms appear to include three components representing three different time scales: sub-weekly, monthly and annual scales. Mismatches between simulated and observed values are analysed as (i) wrong quantification of inputs to the river (especially during the rainy period: combined sewer overflow (CSO), waste water treatment plant (WWTP) and tributary contributions to the nitrate fluxes in the Seine River) and (ii) wrong description of physical processes within the river. Finally, the modelling of simple and cross-variograms appears to be a sensitive analysis tool which can be used to describe and reduce modelling uncertainties. Copyright © 2010 John Wiley & Sons, Ltd.

KEY WORDS river water quality; distributed physically based model; geostatistics; variogram; cross-variogram; uncertainty; validation; nitrate

Received 18 December 2009; Accepted 13 July 2010

INTRODUCTION

The quantitative modelling of in-stream water quality began with a simple conceptual model (Streeter and Phelps, 1925), which was based on oxygen. After this initial step, carbon cycle and then nutrients were added, leading to modern water quality models (Barnwell *et al*., 1987; Brown and Barnwell, 1987; Ambrose *et al*., 1988, 1996; Billen and Servais, 1989; Crabtree *et al*., 1994; Reichert, 1994; Garnier *et al*., 1995; Ivanov *et al*., 1996; Even *et al*., 1998, 2004; Wells, 2000; Wool, 2001). Contrary to the conceptual model by Streeter and Phelps (1925), the biogeochemical processes are nowadays physically based and the transport is based on hydraulic fluxes. Hydraulics can be physically based or conceptual. Reichert *et al*., (2001b) and Arheimer and Olsson (2003) reviewed many of these models.

Even though all these models are more detailed, the distribution through space and the way in which phenomena are described fit a large number of parameters. If the model is based on physical (elementary) processes, some parameter values can be obtained through *in situ* or lab experiments and then physiological parameters are set to these values (Garnier *et al*., 1995; Flipo *et al*., 2007b). But modern biogeochemical models are so complex that they remain difficult to fit and validate (Arhonditsis and Brett, 2004).

The main problem with validating a distributed physically based model (DPBM) is summarized by the equifinality concept (Beven, 1989). As stated by Ebel and Loague (2006) the equifinality is, in the most general sense, the case where quite different processes produce a similar effect. This is because very few measurements are available to mathematically close the system of equations that describes the behaviour of the system. As a consequence, not all unknowns can be identified. This has motivated authors to investigate uncertainty sources which are usually identified as being:

- errors in data used as model inputs;
- errors in validation data, compared with model outputs;
- uncertainties due to sub-optimal parameter values;
- uncertainties due to internal model variability.

These problems remain unsolved even today although many studies have been carried out, leading to interesting uncertainty assessment tools (Refsgaard, 1997; Anderton *et al*., 2002a,b; Butts *et al*., 2004). But, as stated by Beven (2006b): 'there are different philosophies about how to estimate uncertainties and take into account input, measurement and model structural error. These will be difficult to resolve in the near future because we do not actually have the data to properly test the different methodologies'. Even worse, (Beven, 2006b)

* Correspondence to: Edwige Polus, MINES ParisTech, Centre de Geosciences, 35 rue Saint-Honoré, 77305 Fontainebleau, France.
E-mail: edwige.lefebvre@mines-paristech.fr

Copyright © 2010 John Wiley & Sons, Ltd.

goes on with: 'it is simply not possible to evaluate the statistical characteristics of input data errors or parameter estimation errors'.

To summarize the issue in environmental sciences, on one hand, at the hydrological network scale, too few measurements are available to estimate all the variables of the system of equations and to identify all calibration parameters (those which are not easily measured). On the other hand, the system of equations is physically based, describing the behaviour of variables as best as possible. Instead of rejecting this formularism because of mathematical problems, we propose a new methodology for validating in-stream water quality models, based on observations: geostatistics is used to analyse the spatial and temporal behaviour of the observations and to compare the variability of the observations with that of the simulations. Three arguments motivate this approach.

First, the coupling between geostatistics and the process-based modelling was discussed by Fouquet (2006) and successfully applied by Flipo *et al*., (2007a) to the case of nitrate contamination at the basin scale. It was also used by Casper and Vohland (2008), for assessing spatially distributed evaporation.

Then, combining geostatistics and process-based approaches is much more powerful than using a single objective function usually based on root mean squared error (RMSE) or Nash-Sutcliffe efficiency Nash and Sutcliffe, 1970 for hydrologists. Using only statistical criteria will conceal many spatial and time mismatches between simulations and observations. One classical way to assess model stability based on a single criterion is to make Monte Carlo simulations which have a high computer cost, especially when using a distributed process-based model. This limitation is even worse when using multiple criteria, but it is a valuable tool for identifying relevant model components (Guntner *et al*., 1999). In the particular case of hydrology, although a multi-criteria approach can help to better understand what processes need to be further investigated, it is shown that no part of the parameter space yields optimal simulations for all criteria (Anderton *et al*., 2002a,b).

Finally, combining geostatistics and process-based approaches partially addresses the equifinality problem (Beven, 1993, 2006a,b) in that it directly compares the variabilities (and not the variables themselves) of observations and simulations. But it is clear that this technique does not address the *incommensurability* problem (Beven, 1989), which means that parameters and state variables at the grid points of the model often do not correspond to field-based estimates or observations Ebel and Loague, 2006). As discussed in this article, it also allows boundary condition (BC) issues to be identified and provides a framework where measurement errors and model errors can be addressed together through summarizing tools: temporal variograms of both observed and simulated data.

First, the site of interest (250 km in the downstream part of the Seine River) is briefly described. Then theoretical principles are summarized for a process-based modelling of river water quality, as well as geostatistical tools such as variogram and co-kriging. Afterwards a method based on multiple variogram analysis, aiming at assessing the consistency of process-based model outputs with regard to data, is presented and applied to nitrate transfer in the Seine River. Finally, the contribution of this work for reducing model uncertainties is summarized.

MODEL AND DATA OF THE DOWNSTREAM PART OF THE SEINE RIVER

Modelled Area: The Seine River

The studied domain consists in the 225-km stretch along the Seine River and the 36-km stretch along the Marne River. The length of the Seine River upstream of its confluence with the Marne River is approximately 14 km (Figure 1). The Seine and Marne upstream limits

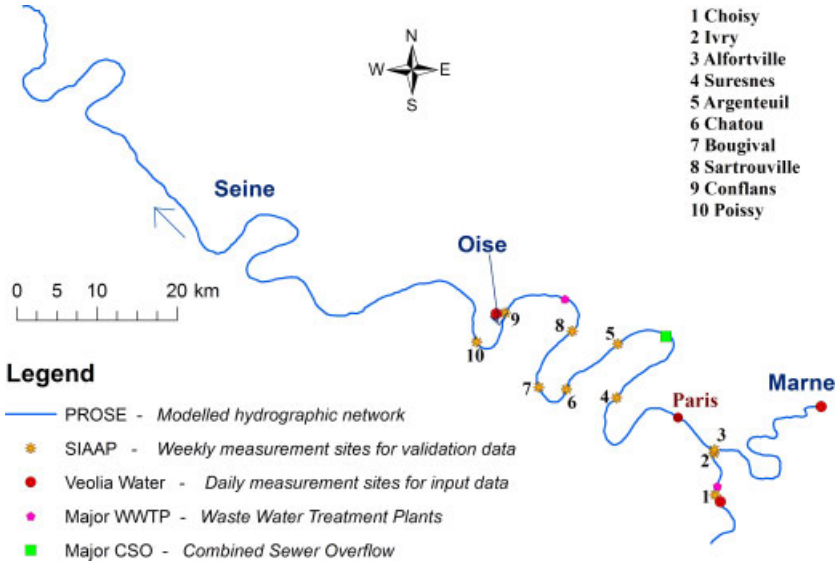

Figure 1. Modelled area and location of different measurement sites

Copyright © 2010 John Wiley & Sons, Ltd.

are located approximately at the entrance of the Greater Paris, whereas the downstream limit is the entrance of the Seine estuary. Two waste water treatment plants (WWTPs), namely Seine Amont and Marne Aval, are located at the upstream limit of the Greater Paris, whereas the Seine Aval WWTP is located close to the downstream limit of the Greater Paris.

The Seine Amont WWTP treats the waste waters from 1 800 000 inhabitants. Its usual discharge is 7 m^3 s^{-1} and up to 17 m^3 s^{-1} during rainy periods. The Marne Aval WWTP treats the waste waters from 220 000 inhabitants. Its usual discharge is 0·9 m^3 s^{-1}. Seine Aval WWTP treats the waste waters from 5 000 000 inhabitants. Its usual discharge is 20 m^3 s^{-1} and up to 50 m^3 s^{-1} during rainy periods. In order to characterize dilution, these WWTP discharge values have to be compared with the Seine discharge in Paris city and at the output of the Seine River when it reaches the Seine estuary. The Seine River mean discharge in Paris is 280 m^3 s^{-1}, decreasing to 60 m^3 s^{-1} in summer with a 5-year return period. At the entrance of the estuary, the Seine River mean discharge is 540 m^3 s^{-1} decreasing to 180 m^3 s^{-1} in summer with a 5-year return period.

The total length of the Seine River in this large urban area is approximately 80 km. Recently, the ProSe model was used to simulate the water quality for the 2003–2008 period. This study focuses on the year 2003, and on nitrate.

The ProSe model

The ProSe model (Even *et al*., 1998, 2004; Flipo *et al*., 2004) is composed of three modules (Figure 2a): hydrodynamic, transport and biogeochemical modules.

The hydrodynamic module is based upon a longitudinal 1D form of the Saint-Venant equations, solved by the finite difference method. The transport module simulates the advection and dispersion of conservative and reactive substances, both particulate and dissolved.

The biogeochemical model is an adaptation of the RIVE model (Billen *et al*., 1994; Garnier *et al*., 1995) (Figure 2b); it is described in Appendix A. For modelling purposes, the river is divided into three compartments (Figure 2a): the water column, the sediments and the periphyton, integrating both the epilithon and the epipelon. The water column can, through sedimentation, erosion, permanent loses and scouring, exchange suspended matter with sediment and periphytic layers (Flipo *et al*., 2004). Two compartments were simulated (water column and sediments) because biogeochemical reactions due to periphyton are less important in large rivers than in headwater streams (Flipo *et al*., 2004, 2007b).

As the aim of this study is to simulate nitrate concentrations in the water column, we focus only on processes affecting the nitrogen concentration hereafter. ProSe outputs are instantaneous values of local nitrate concentrations at each cell center.

Model calibration and validation. The conceptual scheme of RIVE is based on a macroscale simulation of the micro-organism dynamics that govern the transformation of many constituents (organic matter, nutrients and oxygen). The main idea is that the biological processes are always the same but stimulated differently according to different environmental conditions, which leads to different states of the hydrosystem (Reichert *et al*., 2001b,c; Billen *et al*., 2005). The main part of the physiological parameters of primary producers (PPs) and bacteria has been determined experimentally on natural assemblages of phytoplankton or bacterioplankton (Billen *et al*., 1990b; Garnier *et al*., 1995, 1998), or based on a literature review or fitted by trial-errors in previous studies (Garnier *et al*., 1995, 2000; Even *et al*., 1998, 2004;

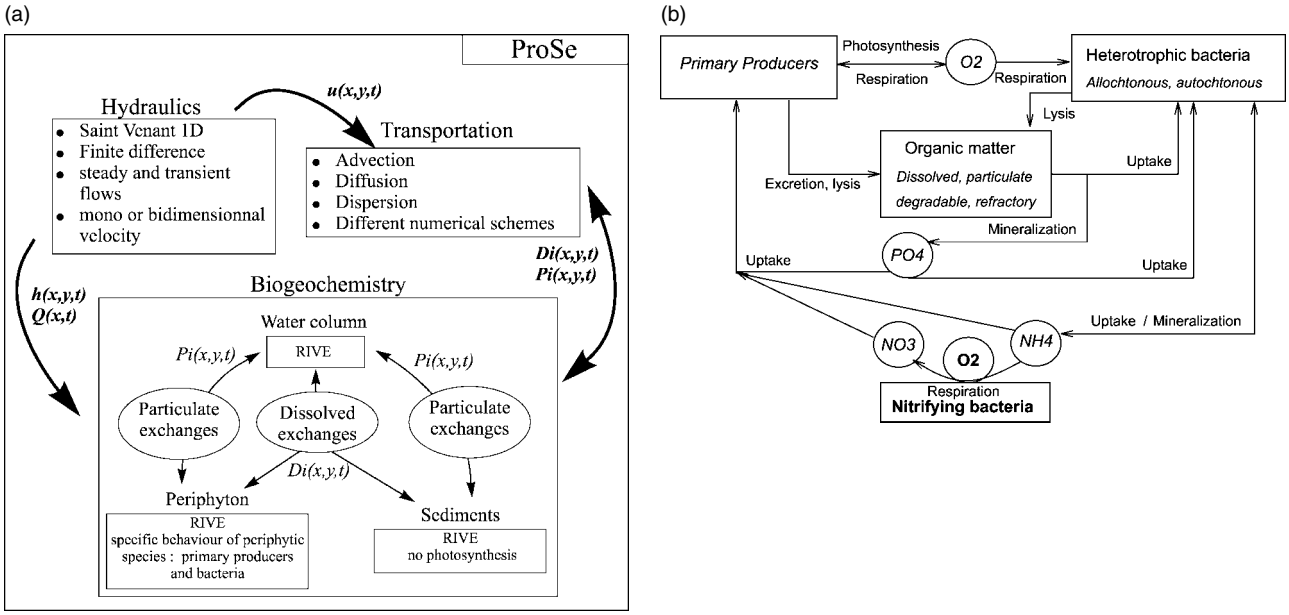

Figure 2. (a) Simplified scheme of the ProSe model. h is the water depth, u the velocity, Q the discharge, D_i and P_i are dissolved and particulate phases of the i-species. (b) Simplified scheme of the RIVE model. Carbon, oxygen and nutrient cycles are represented

Copyright © 2010 John Wiley & Sons, Ltd.

Flipo *et al*., 2004). Hydrodynamical and transport parameters have also been fitted by trial-errors for ProSe (Even *et al*., 1998, 2004) or for other models (Billen *et al*., 1994; Garnier *et al*., 1995; Garnier, 2000). Then the rive model has been successfully applied to many rivers of the Seine basin (Garnier *et al*., 1995, 2005; Billen *et al*., 1998b, 2001; Even *et al*., 1998, 2007a; Sferratore *et al*., 2005; Flipo *et al*., 2007b,c) and of other basins, including the Danube (Garnier *et al*., 2002), the Schelde (Billen *et al*., 2005) and the Red River (Quynh, 2005).

BCs and model parameterization are briefly commented hereafter. They are described in detail by (Poulin (2006).

Measurements

The two data sets of nitrate concentrations used in this study were obtained from different measurement techniques.

Input data. The water supplier, Veolia Water, provides data sets which consist of daily concentrations, with some of them averaged from hourly measurements. Three measurement sites (Figure 1) are located at the upstream part of each modelled river (Seine and Marne) and at the confluence of the Seine River with the Oise River, which is not modelled by ProSe. These three data sets are used as upstream BCs.

Validation data. For the year 2003, the Sewage Public Company of the Greater Paris (SIAAP) provided weekly measurements at ten sampling sites (Figure 1): one on the Marne River and nine on the Seine River. For the sites where a lateral heterogeneity is observed, a measurement value consists, in the average, of three samples taken from the left side to the right side of the river. This average value on a cross section allows a longitudinal 1D description to be made.

COMBINING GEOSTATISTICS AND PHYSICALLY BASED MODELLING

Geostatistical tools: variogram and bivariate model

Some basic principles of geostatistics used in the following are briefly given in the temporal context (1D). For further developments (and the usual spatial case), one may consult (Chiles and Delfiner, 1999).

Temporal variogram. The variogram quantifies the temporal variability of a variable. Let $Z(t)$ be the value of the Z variable at the instant t. The temporal variogram $\gamma(\tau)$ is defined as half the probabilistic mean (or mathematical expectation, noted E), of the squared differences between $Z(t+\tau)$ and $Z(t)$, as a function of the time interval τ (Equation 1).

$$\gamma(\tau) = \frac{1}{2}E[(Z(t+\tau) - Z(t))^2] \quad (1)$$

By definition, $\gamma(0) = 0$. Generally, the magnitude of the increment $Z(t+\tau) - Z(t)$ increases with τ. If Z fluctuates around a constant mean, the mean of these increments is zero, which is the reason why squared differences $(Z(t+\tau) - Z(t))^2$ are used. If the amplitude of the fluctuations is almost constant, then the random function (RF) Z is stationary (of order 2) and the variogram stabilizes around a 'sill' beyond a maximal correlation distance called 'range'.

In practice, data are available only at experimental points, from which an experimental variogram $\gamma^*(\tau)$ is calculated (*cf* section on *Introduction to geostatistics* in Appendix B). This experimental variogram is then fitted by a theoretical variogram function, with the appropriate mathematical properties (Chiles and Delfiner, 1999).

Typically, variogram $\gamma(\tau)$ can be decomposed as the sum of several components, e.g. $\gamma(\tau) = \gamma^0(\tau) + \gamma^1(\tau) + \gamma^2(\tau)$, where γ^0 admits a null range (nugget effect), γ^1 admits a range a_1 and γ^2 admits a greater range a_2. For a phenomenon presenting a periodical component, the variogam admits a sinusoidal component with the same period as the phenomenon.

The cross-variogram describes the joint variability of two variables Z_1 and Z_2. It is defined as half the covariance of increments according to the time interval τ:

$$\gamma_{12}(\tau) = \frac{1}{2}E[(Z_1(t+\tau) - Z_1(t)).(Z_2(t+\tau) - Z_2(t))] \quad (2)$$

Unlike the 'simple' variogram, the cross-variogram can be negative when both variables, and thus their increments, are negatively correlated. When there is no temporal cross-correlation between Z_1 and Z_2 (they are temporally cross-uncorrelated), then their cross-variogram is null: $\gamma_{12}(\tau) = 0$.

Estimation: kriging and its variants. Among estimators built as a linear combination of data, kriging is defined by the following properties:

- no bias (on average, the estimation error is null);
- 'optimality': the variance of the estimation error is minimal (in other words, the precision is as best as possible).

The multivariate version of kriging is co-kriging, which consists in estimating Z_1 from measurements of Z_1 and Z_2. Let us assume that $\gamma_{12}(\tau) \neq 0$ and thus that Z_1 and Z_2 are temporally cross-correlated. If Z_2 is denser sampled than Z_1, then data of Z_2 can be used to interpolate the missing values of Z_1, with respect to the probabilistic relationship between Z_1 and Z_2. The minimization of the estimation error variance under non-bias conditions leads to a linear system that involves simple and cross-variograms of the different variables: $\gamma_1(\tau)$, $\gamma_2(\tau)$ and $\gamma_{12}(\tau)$ (section on *Estimation by co-kriging* in Appendix B).

Geostatistical bivariate model: understanding how variables are linked. Fitting simple and cross-variograms

Copyright © 2010 John Wiley & Sons, Ltd.

is a way to model the link between variables. One way to understand the differences between simulations and observations is thus to analyse the fitting of their simple and cross-variograms. The geostatistical bivariate model used in this article is a very general one, the linear model of co-regionalization.

Let $O(t)$ be the observations and $S(t)$ the simulated values. In this model, both variables can be divided into n components $O_i(t)$ and n components $S_i(t)$ (Equation 3).

$$\begin{cases} O(t) = \sum_{i=1}^{n} O_i(t) \\ S(t) = \sum_{i=1}^{n} S_i(t) \end{cases} \tag{3}$$

$\forall i \neq j$, $O_i \perp O_j$, $S_i \perp S_j$, $O_i \perp S_j$, where $\perp$ means that the different components are temporally uncorrelated, i.e. their temporal cross-covariance (or variogram) is zero: $\forall i \neq j$, $\forall t$, $\forall t'$, $Cov(O_i(t), O_j(t')) = 0$, written $O_i \perp O_j$.

The link between variables is described by the correlation between the n couples of components O_i and S_i. For a given i, O_i and S_i are possibly correlated, which can be written:

$$\exists\, \omega_i,\ \rho_i, \quad and \quad R_i \perp S_i \mid O_i(t) = \rho_i\, \omega_i\, S_i(t) + \omega_i \sqrt{1-\rho_i^2}\, R_i(t) \tag{4}$$

where ω_i^2 is the 'sill ratio' of $\gamma_O^i(\tau)$ and $\gamma_S^i(\tau)$, ρ_i is the correlation coefficient between O_i and S_i at the same instant t, and $R_i(t)$ is an RF temporally uncorrelated to $S_i(t)$, with a variogram proportional to the one of S_i.

Equation 4 implies that $\gamma_O^i(t) = b_{OO}^i \gamma_i(t)$, $\gamma_S^i(t) = b_{SS}^i \gamma_i(t)$ and $\gamma_{OS}^i(t) = b_{OS}^i \gamma_i(t)$, with $b_{OS}^i \leq \sqrt{b_{OO}^i\, b_{SS}^i}$. Thus, $\omega_i^2 = \dfrac{b_{OO}^i}{b_{SS}^i}$ and $\rho_i = \dfrac{b_{OS}^i}{\sqrt{b_{OO}^i\, b_{SS}^i}}$

Figure 3 illustrates three specific versions of the linear model of co-regionalization (*cf* section on *Geostatistical bivariate models* in Appendix B) that will be found hereafter.

1. The residual model: the observations are the sum of the simulations and of another term R, which is independent of these simulations: $S \perp R$
2. The intrinsic correlation model: simple and cross-variograms are proportional to each other. The strength of the correlation between simulations and observations is given by the sill of the cross-variogram: the higher it is the stronger is the correlation. This model was already used by Chiles and Vohland (2008) to compare measurements to a physically based model of air pollution
3. The linear model of co-regionalization: each component i corresponds to the intrinsic correlation, but the combination of these components does not correspond to an instrinsic correlation (i.e. for $i \neq j$, $\rho_i \neq \rho_j$ or $\omega_i \neq \omega_j$). The analysis of relationships between variables must then be performed for each component separately.

Physics-based simulations

For this work, ProSe was run for the whole year 2003, simulating water quality on the domain (*cf* section on *Modelled area: the Seine River*) from the 1st of January to the 31st of December.

River discharges and urban hydrology. Daily river discharges were used for the Seine, Marne and Oise Rivers and for the minor tributaries. For the Seine and Marne Rivers, the upstream discharges are available. For the other tributaries, the discharge is measured or estimated close to their confluence with the Seine River. WWTP outflows and combined sewer overflows (CSOs) are measured values or estimates provided by the SIAAP. The hydraulic model describes the variation of discharge along the domain. During low discharge periods, the residence time of water might be as long as 1 month since the Seine and Marne Rivers are regulated for navigation purposes by 14 dams. At the outlet of the modelled domain, the comparison of the calculated and measured downstream discharges demonstrates that the transient

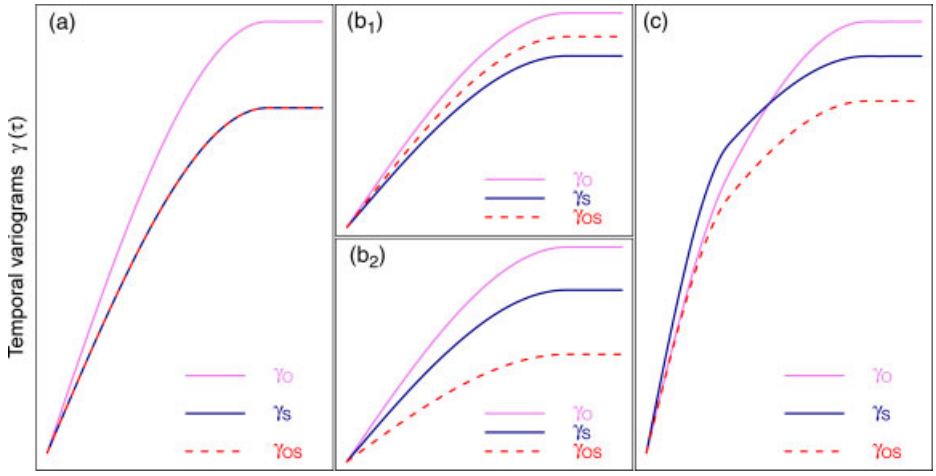

Figure 3. Possible relationships between temporal simple and cross-variograms of observations O and simulations S. (a) Residual model; (b) Intrinsic correlation model; (c) Linear model of co-regionalization (*cf* section on *Geostatistical bivariate models* in Appendix B for more details)

Copyright © 2010 John Wiley & Sons, Ltd.

water balance is estimated with a good precision for the whole domain as well as the residence time for low or high discharges (Polus-Lefebvre *et al.*, 2008).

Boundary conditions. The model requires BCs for each major tributary. For the Seine and the Marne Rivers, BCs are necessary at the upstream point of the modelled domain. The third river (the Oise River) and the four minor tributaries are not modelled, so BCs are defined at their confluence with the Seine River. BCs for minor tributaries are composed of daily mean values of discharge and monthly values (one sample per month) of water quality variables. The Seine, Marne and Oise BCs are daily concentrations of all modelled variables provided by Veolia Water (*cf* section on *Input data*). They are called *initial BCs* in the rest of the article.

Statistical and geostatistical criteria for comparison

Validation data ($O(t_i)$) and ProSe outputs ($S(t_i)$) are compared for both simulations. Statistical criteria are first calculated: average, standard deviation on variables and on residuals ($\varepsilon(t_i) = S(t_i) - O(t_i)$ (Eq. 5)), and as RMSE between time series $O(t_i)$ and $S(t_i)$ (Eq. 6). RMSE quantifies averaged squared differences between model and data 'point by point', at the same days.

$$\sigma = \sqrt{\frac{1}{n}\sum_{i=1}^{n}(\varepsilon(t_i) - \overline{\varepsilon})^2} \tag{5}$$

$$RMSE = \sqrt{\frac{1}{n}\sum_{i=1}^{n}\varepsilon^2(t_i)} \tag{6}$$

In addition, temporal simple and cross-variograms are used to compare the variability of modelled and measured nitrate concentrations. Simple variograms indicate whether the modelled variability is consistent with the experimental data variability. Cross-variogram between modelled and data time series shows how they are temporally correlated. Particular attention is given to the coefficients ρ_i and ω_i for each variogram component (section on *Geostatistical bivariate model: understanding how variables are linked*).

In order to calculate simple and cross-variograms in the same conditions, ProSe outputs are sampled according to SIAAP measurement days; it means a weekly sampling, assuming that measurements are made at noon. All presented variograms are thus calculated from instantaneous weekly sampled concentrations.

RECONSTRUCTING BC BY CO-KRIGING

Preliminary exploratory analysis

First comparison concerns ProSe values and SIAAP measurements of nitrate concentrations. For most of the year, measured nitrate concentrations appear to be lower than ProSe values at almost all sites. Figure 4a summarizes this analysis by presenting the evolution along the Seine River of average differences at each site between simulated and measured nitrate concentrations over the whole year. A systematic deviation is pointed out from upstream of the domain to at least the Sartrouville site.

Two nitrate time series are available upstream of the Seine River: daily Veolia measurements used as input data and weekly SIAAP measurements at Choisy (*cf* section on *Measurements*). Both time series are compared visually (Figure 4b) and statistically (Table I); both present an annual periodicity and a high temporal correlation (*cf* Figure 4b, correlation coefficient = 0·89). But most nitrate concentrations measured by the SIAAP appear to be lower than those measured by Veolia Water.

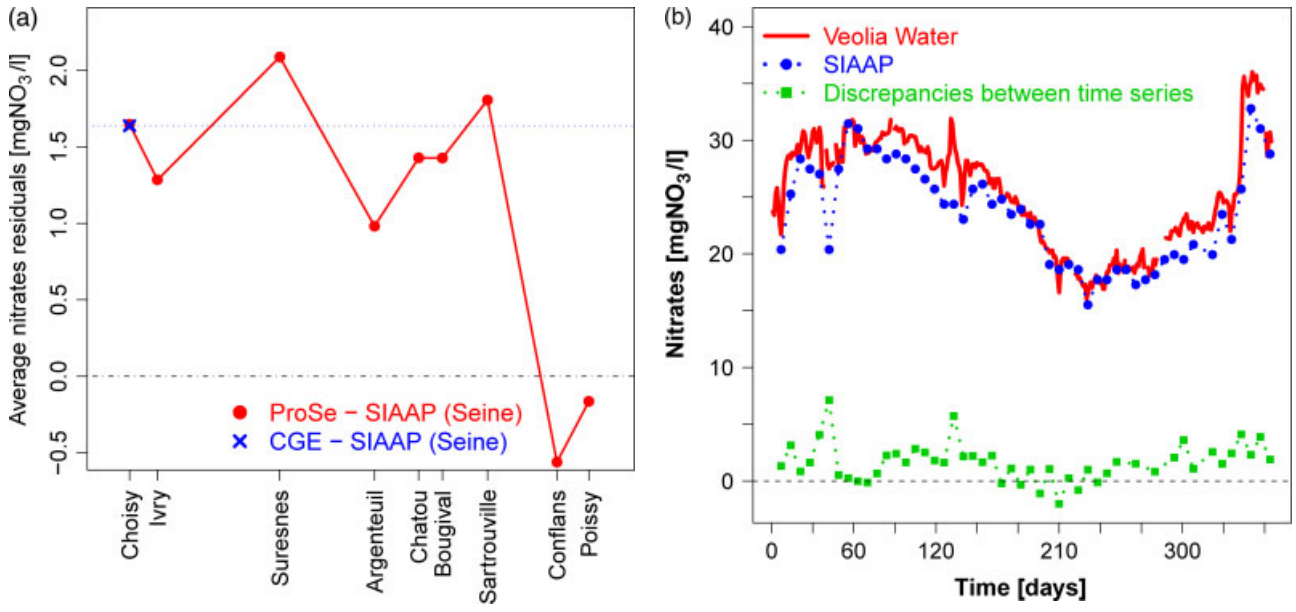

Figure 4. (a) Average deviations of nitrate concentrations between ProSe values and SIAAP measurements. (b) Comparison of nitrate concentrations upstream of the Seine River: validation data (SIAAP), input data (Veolia Water), and discrepancies between both time series

Copyright © 2010 John Wiley & Sons, Ltd.

Table I. Statistics on nitrate concentrations [mg NO_3 l^{-1}] in Choisy: validation data (SIAAP), input data (Veolia Water), and discrepancies between both time series; the correlation coefficient between time series is 0·89

	m	σ^2	σ	Min.	Max.
Observed nitrates (SIAAP)	23·6	20·2	4·5	15·5	32·8
Initial BC (Veolia Water)	25·5	23·3	4·8	16·0	36·0
Discrepancies	1·6	2·8	1·7	−2·0	7·1
Modified BC	23·7	19·0	4·4	15·5	33·0

m stands for the average, σ^2 for the variance and σ for the standard deviation. Comparison of initial and modified BCs.

More specifically, discrepancies are close to zero in summer (days 170–240), but during the rest of the year they are more significant and can reach 7 mg NO_3 l^{-1}, i.e. a relative deviation of more than 20%.

Discrepancies between Veolia Water and SIAAP measurements can be explained by different measurement protocols and sampling strategies (*cf* section on *Measurements*). Nevertheless it is difficult to know which values are closer to reality. We decided to give the preference to SIAAP measurements because they are consistent with downstream measured values and with the monthly values given by the administration in charge of water quality control.

Reconstruction principle

In order to avoid deviations due to sampling and methodology differences and to improve the consistency between ProSe outputs and observed (SIAAP) nitrate concentrations, we decided to modify the nitrate Seine BCs. Instead of daily measurements operated by Veolia Water, SIAAP measurements at Choisy are considered for BCs in the Seine River. But anyhow, BCs must be daily concentrations, whereas SIAAP data are weekly available.

The temporal co-kriging (*cf* sections on *Geostatistical tools: variogram and bivariate model* and *Estimation by co-kriging* in Appendix B) of weekly SIAAP measurements by daily Veolia Water measurements uses at best the cross-correlation between both time series to provide a daily time series:

- that perfectly fits SIAAP measurements;
- with the daily variability of Veolia Water measurements.

The co-kriging is thus performed assuming that the temporal variability of daily values is identical at both SIAAP (Choisy) and Veolia Water sites, located 9 km from each other. The approximation, which consists in neglecting this distance, seems reasonable since the spatial variability of nitrate concentrations is much lower than their temporal variability (Polus-Lefebvre *et al.*, 2008).

Co-kriging

First, a bivariate linear model of co-regionalization is fitted to simple and cross-variograms of SIAAP and Veolia Water measurements (Figure 5a). The resolution of the linear system developed in the section on *Estimation by co-kriging* in Appendix B gives the co-kriging weights. The resulting time series (Figure 5b) exactly fits the experimental SIAAP measurements and its variability is similar to that of Veolia Water measurements.

The same method was applied to the Oise River (*cf* Figure 1), given that SIAAP measurements are available downstream of the Oise River. From now on, these two reconstructed daily time series are called *modified BCs*.

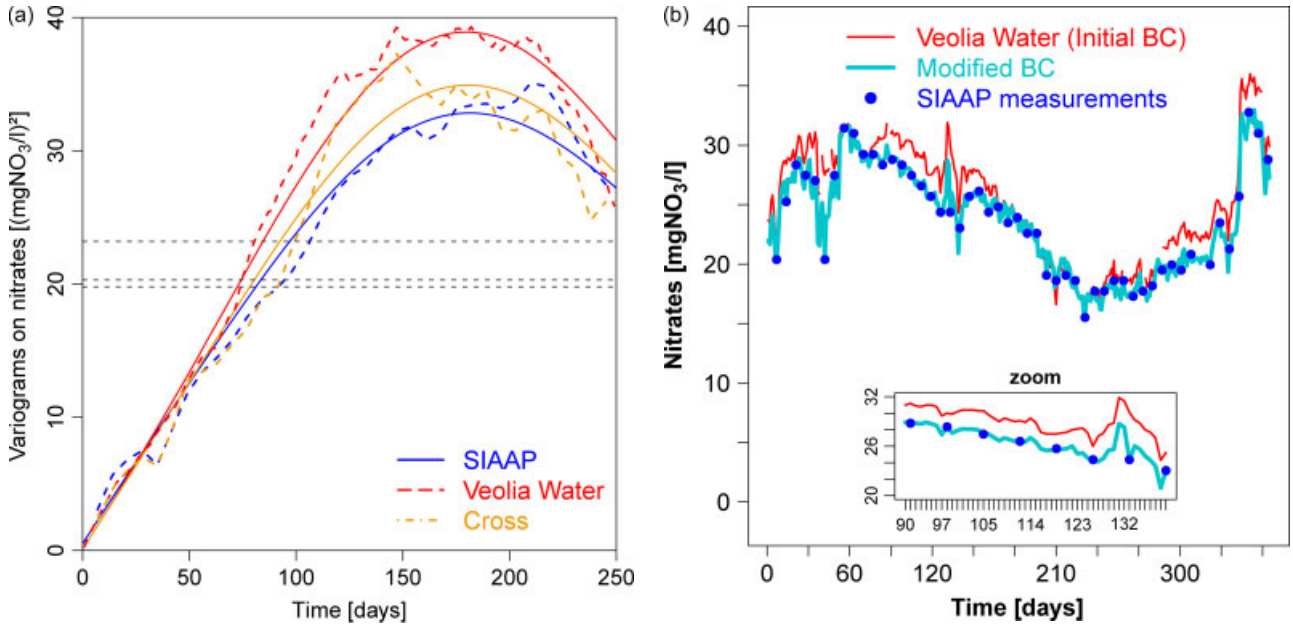

Figure 5. (a) Experimental and fitted variograms of nitrate concentrations upstream of the Seine River. (b) Comparison of nitrate time series used as BC: Veolia Water data for simulation 1 (Initial BC) and time series reconstructed by co-kriging for simulation 2 (Modified BC)

Copyright © 2010 John Wiley & Sons, Ltd.

It was not possible to reconstruct consistent BCs for the Marne River. Indeed the unique measurement site providing validation data is located more than 30 km downstream of the upper limit where daily input data are needed. We have considered that it would not be consistent to use a reconstructed time series passing through experimental points that are too far. Thus, Marne River BCs remained unchanged.

A second ProSe simulation was run with the *modified BCs* obtained from co-kriging for nitrate concentrations upstream of the Seine and the Oise Rivers. All other BCs remain unchanged.

Comparing simulations with initial and modified BCs to measured nitrate

With modified BCs, simulated nitrate concentrations are more consistent with validation data (Figure 5b and 6). The averaged deviation on the domain drops from 1·1 mg NO_3 l^{-1} to 0·1 mg NO_3 l^{-1} (Table II). The average RMSE was also reduced from 2·3 mg NO_3 l^{-1} to 1·8 mg NO_3 l^{-1} when considering the modified BCs (Table II).

In general, the simulation with modified BCs gives better results than the one with the initial BC (Table II and Figure 7). This is the case for all SIAAP sites up to the junction with the Oise River. From there, statistical criteria are better for the simulation with initial BCs, and ProSe slightly underestimates nitrate concentrations at Conflans and Poissy where the average errors of estimate are $-1{\cdot}2$ mg NO_3 l^{-1} and $-0{\cdot}7$ mg NO_3 l^{-1}, respectively, for the simulation with modified BCs (Table II). Based only on statistics, one could guess that this is due to underestimated fluxes in the Oise River. But looking more carefully at time series (Figure 7), one can see that ProSe outputs start to slightly diverge from observations from day 150. One explanation might be that either denitrifying bacteria dependency on temperature is overestimated in the model (the summer of 2003 was unusually dry and warm in France) or that sediment accumulation is overestimated by the model in this part of the network.

In the remaining of the article, we will thus analyse simulation outputs obtained with modified BCs, which show a better agreement with observed data.

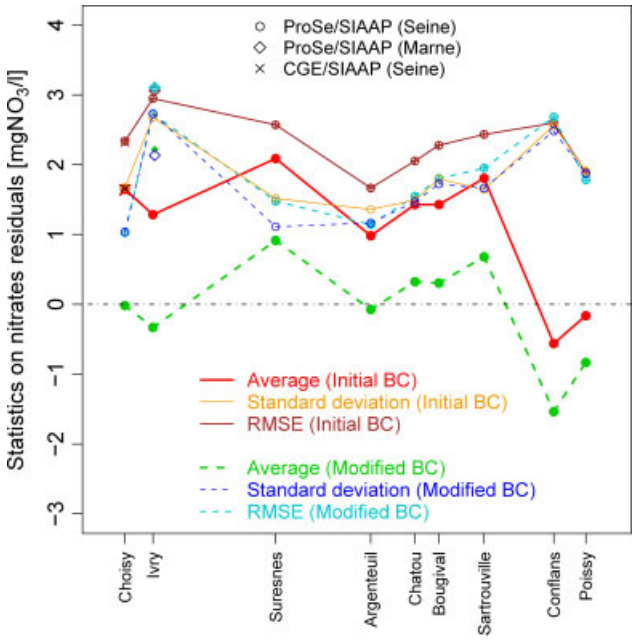

Figure 6. Statistics on deviations of nitrate concentrations between ProSe values and SIAAP measurements from upstream to downstream; comparison of initial and modified BC

Table II. Statistics on deviations of nitrate concentrations [mg NO_3 l^{-1}] between ProSe values and validation data (SIAAP), and RMSE between both time series

	m_1	m_2	σ_1	σ_2	$RMSE_1$	$RMSE_2$
Choisy	1·7	−0·0	1·7	1·0	2·3	1·0
Ivry	1·3	−0·3	2·7	2·7	2·1	2·7
Suresnes	2·1	1·0	1·5	1·1	2·6	1·5
Argenteuil	1·0	0·0	1·4	1·2	1·7	1·1
Chatou	1·4	0·5	1·5	1·5	2·1	1·6
Bougival	1·4	0·5	1·8	1·8	2·3	1·8
Sartrouville	1·8	0·9	1·7	1·8	2·4	2·0
Conflans	−0·6	−1·2	2·6	2·4	2·6	2·7
Poissy	−0·2	−0·7	1·9	1·7	1·9	1·8
Average	1·1	0·1	1·9	1·7	2·3	1·8

m stands for the average and σ for the standard deviation. Comparison of simulations with initial ('1') and modified ('2') BCs at all validation sites.

RESULTS AND DISCUSSION

First, ProSe outputs are compared to validation data using usual statistical tools, then a more detailed analysis involving geostatistical tools is presented.

Classical result analysis

First, statistical criteria (*cf* section on *Statistical and geostatistical criteria for comparison*) are used to compare ProSe values to SIAAP measurements at each validation site (Table III), complementary to visual comparison that can be made on Figure 7. As seen when comparing inital and modified BCs, the annual mean nitrate concentration is well estimated by ProSe at each validation site, with small differences, either positive or negative. The temporal variability is slightly underestimated by the model at almost all sites, ProSe values presenting standard deviations ranging from 3·3 to 4·5 mg NO_3 l^{-1} against a range from 3·7 to 4·5 mg NO_3 l^{-1} for SIAAP measurements. Moreover, the correlation coefficients are very high ($\rho > 0{\cdot}9$) and RMSE (*cf* Equation 6) are close to 1, except at Ivry ($\rho = 0{\cdot}74$ and $RMSE =$ 2·7 mg NO_3 l^{-1}) and Conflans ($\rho = 0{\cdot}84$ and $RMSE =$ 2·7 mg NO_3 l^{-1}).

The statistical criteria and the visual comparison of simulated and observed nitrate concentrations lead to the same conclusion: nitrate seems well simulated by the ProSe model for the year 2003.

Copyright © 2010 John Wiley & Sons, Ltd.

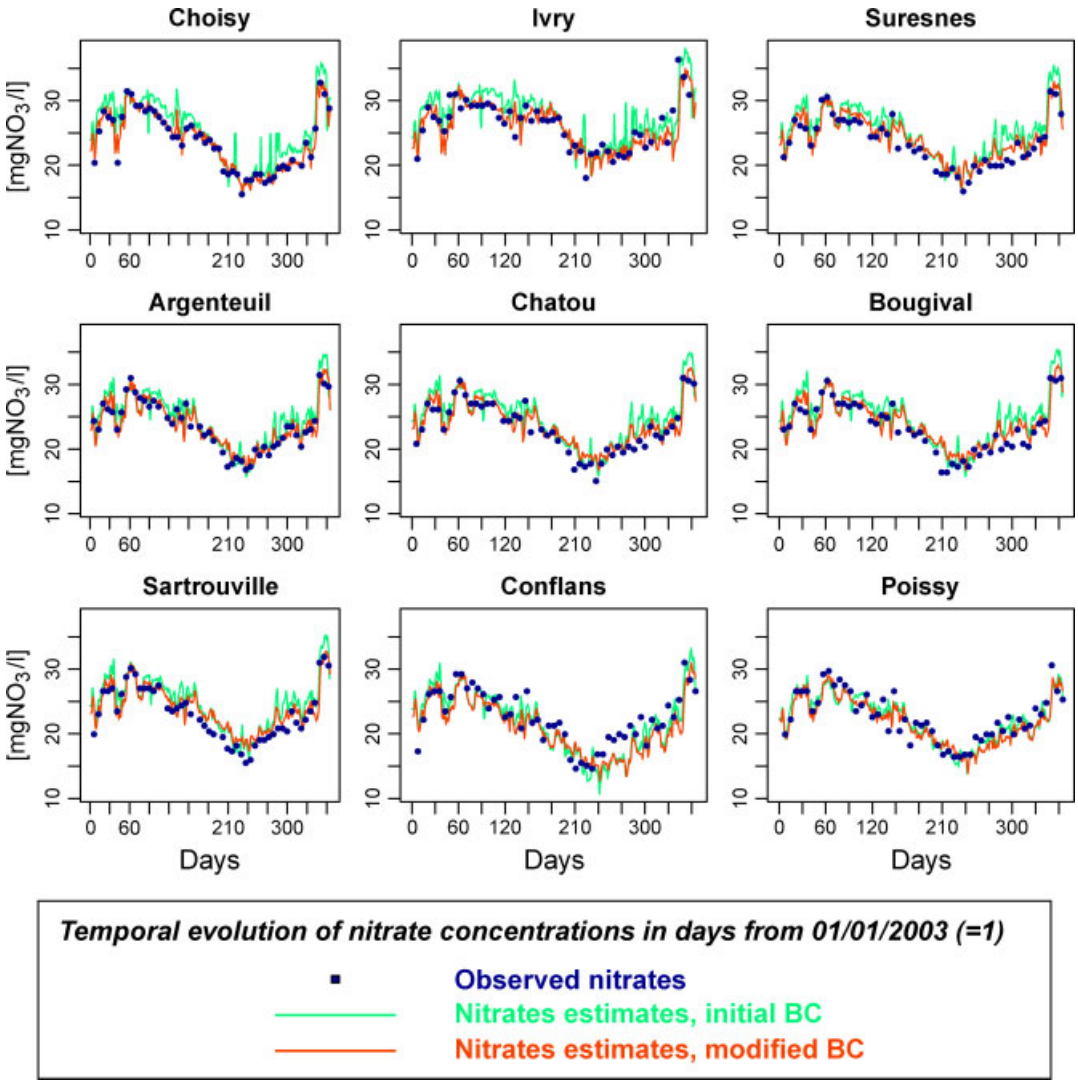

Figure 7. Comparison of modelled (ProSe) and measured (SIAAP) nitrate concentrations in 2003 at each measurement site. The two simulations with different BC are also compared. All sites are presented from upstream (Choisy) to downstream (Poissy) along the Seine River

Table III. Statistics on nitrate concentrations [mg NO_3 l^{-1}] in all validation sites: comparison of ProSe values and SIAAP measurements

Site	SIAAP		ProSe			
	m	σ	m	σ	ρ	RMSE
Choisy	23·6	4·5	23·6	4·5	1·0	1·0
Ivry	26·2	3·7	25·8	3·7	0·7	2·7
Suresnes	23·5	3·8	24·3	3·3	1·0	1·5
Argenteuil	23·6	3·9	23·6	3·8	1·0	1·1
Chatou	23·4	4·0	23·7	3·7	1·0	1·6
Bougival	23·4	3·9	23·8	3·6	0·9	1·8
Sartrouville	23·1	4·2	23·8	3·5	0·9	2·0
Conflans	22·4	4·1	20·8	4·4	0·8	2·7
Poissy	22·6	3·7	21·7	3·7	0·9	1·8

m, σ, ρ, and *RMSE*, respectively stand for mean, standard deviation, correlation coefficient and RMSE.

Result analysis using fitted variograms

The observed and the ProSe simple and cross-experimental variograms are fitted at each gauging site with a linear model of co-regionalization. The corresponding simple and cross-modelled variograms are called γ_O, γ_S and γ_{OS}, respectively (Figure 8 and Table IV).

The linear model of co-regionalization is a combination of the following three components:

- a nugget effect which integrates sub-weekly variability and sampling uncertainty. It accounts for less than 5% of the total variance at each gauging station;
- an exponential variogram which corresponds to a decreasing correlation with time increase. For every site, a range of about 1 month is observed. It accounts for around 20% of the total variance;
- a periodic component with an annual period. This is the major component since it accounts for around 75% of the total variance. This periodical structure is consistent with the seasonal variability observed on time series (Figure 7), which might be related to bacterial activity and temperature annual variations: denitrification activity is the highest in late summer due to high water temperature. The annual minimum

Copyright © 2010 John Wiley & Sons, Ltd.

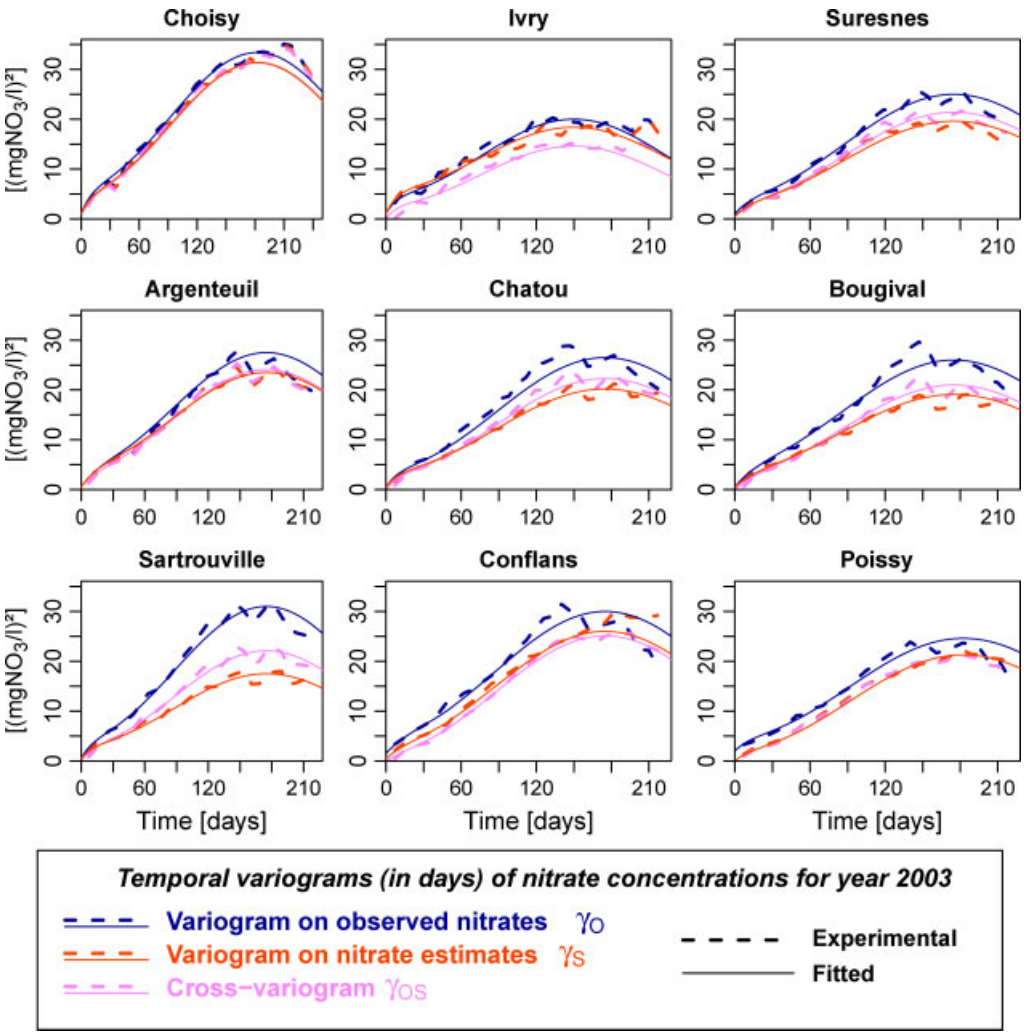

Figure 8. Fitted temporal simple and cross-(γ_{OS}) variograms of measured (SIAAP, γ_O) and modelled (PROSE, γ_S) nitrate concentrations at each measurement site, with a linear model of co-regionalization

Table IV. Fitting of variograms composed of three terms: nugget effect, exponential component and periodic component

Gauging station		Nugget effect			Exponential			Periodic (cosinus)			Global sill		
		γ_{obs}	γ_{prose}	γ_{cross}	γ_{obs}	γ_{prose}	γ_{cross}	γ_{obs}	γ_{prose}	γ_{cross}	γ_{obs}	γ_{prose}	γ_{cross}
Choisy	Sill $[(mg\ l^{-1})^2]$	1	1	0·7	6	5	5	26·4	25·4	25·6	33·4	31·4	31·3
	Range or period* [d]				35	35	35	365	365	365			
Ivry	Sill $[(mg\ l^{-1})^2]$	1	1	0	4	5	3	15	12·4	11·6	20	18·4	14·6
	Range or period [d]				25	25	25	300	300	300			
Suresnes	Sill $[(mg\ l^{-1})^2]$	1	0·5	0·5	4	3·5	3·5	20	15·6	17·4	25	19·6	21·4
	Range or period [d]				40	40	40	350	350	350			
Argenteuil	Sill $[(mg\ l^{-1})^2]$	0·5	0·5	0·5	5	5	4	22	18	19·6	27·5	23·5	24·1
	Range or period [d]				45	45	45	350	350	350			
Chatou	Sill $[(mg\ l^{-1})^2]$	0·5	0·5	0	4	3·5	3·5	22	16·2	18·8	26·5	20·2	22·3
	Range or period [d]				30	30	30	350	350	350			
Bougival	Sill $[(mg\ l^{-1})^2]$	0·5	0·5	0	5·5	5·5	4	20	14·6	17	26	19·1	21
	Range or period [d]				50	50	50	350	350	350			
Sartrouville	Sill $[(mg\ l^{-1})^2]$	0·5	0·5	0	4·5	3	3·5	26	14	18·6	31	17·5	22·1
	Range or period [d]				35	35	35	350	350	350			
Conflans	Sill $[(mg\ l^{-1})^2]$	1·5	0·5	0	4·5	3·5	2·5	24	22	22·6	30	26	25·1
	Range or period [d]				45	45	45	350	350	350			
Poissy	Sill $[(mg\ l^{-1})^2]$	2	0	0	3	2·5	2·5	19·6	18·8	18·8	24·6	21·3	21·3
	Range or period [d]				35	35	35	365	365	365			

γ_{obs}: variogram of measurements; γ_{prose}: variogram of simulated values; γ_{cross}: cross-variogram. * Range for the exponential component and period for the cosinus component.

Copyright © 2010 John Wiley & Sons, Ltd.

observed for nitrate concentrations might also be related to river discharge, which produces dilution. During low water season, nitrate are mainly brought to the rivers from aquifers (where the concentration is stable or in slow evolution), the surface runoff contribution, with higher nitrate concentrations, being negligible at this time. This periodical structure was confirmed at each SIAAP sampling site on 3-year records (from 2001 to 2003) (Figure 9).

Globally, ProSe variograms present similar patterns than the observed ones, but ProSe always underestimates the nitrate temporal variability, with a global sill ratio ranging from 0·57 to 0·94 (Table V). It confirms and reinforces the slight underestimation highlighted in the previous section based on classical statistics.

Fitting a variogram model to experimental variograms provides information about the link between simulated and observed values. Pointing out changes in variogram patterns from upstream to downstream allows modifications of the link between model and mesaurements to be located. Then the 'approximation' (either in processes, parameters or data) responsible for each change can be characterized through the joint analysis of the different components, the time series and the classical statistics.

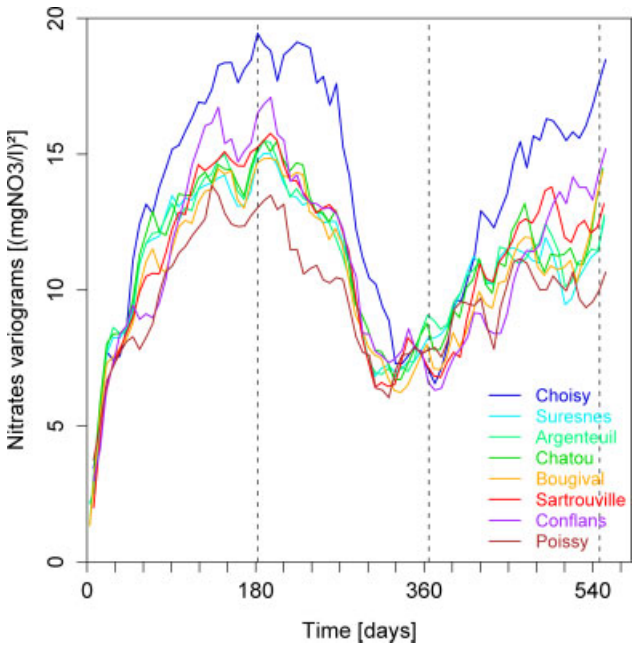

Figure 9. Temporal simple variograms of weekly measured nitrate concentrations by the SIAAP, for the 3 years 2001 to 2003

Before analysing further the variogram changes from upstream to downstream, it is important to keep in mind that for each component of the fitted variograms, the sill ratio between simple variograms gives an indication about the ratio of the fluctuation amplitude. A sill ratio equals to 1 indicates that the amplitude of ProSe temporal fluctuations is similar to that observed. Otherwise, this amplitude is either over (>1) or underestimated (<1). Conversely, the correlation coefficient provides information on the similarity of both series. $\rho = 1$ indicates that both time series evolve similarly, whereas $\rho = 0$ indicates that the time series are not correlated at all.

As BCs were modified to build a consistent dataset, the differences between γ_O and γ_S, as well as the position of γ_{OS}, are due to an inadequate quantification of inputs to the river and to approximations into the description of physical processes within the river (i.e. an approximate description of phenomenon and/or an approximate parameterization of the model, 1D modelling). From upstream to downstream of the modelled area, the variogram patterns evolve as follows (Table IV and V):

From Choisy to Ivry. At Choisy, upstream of the domain, the model works properly: $\gamma_{OS} \approx \gamma_S \approx \gamma_O$. But at Ivry $\gamma_{OS} < \gamma_S < \gamma_O$ and the determination coefficient ρ^2 is only 0·5 ($\rho = 0{\cdot}71$ in Table V). The temporal correlation is the weakest overall in the modelled area, especially for the exponential component and the nugget effect. Among all sites, the sill of γ_O is here the lowest one because of the low sill of the periodic component which is only 15 (mg NO_3 $l^{-1})^2$. ProSe also reproduces the reduction in the global and periodic sills but it overestimates this reduction (Table IV). At Ivry, the range of the exponential component is the lowest one as well (25 days). During spring and winter (around 150 days), nitrate concentrations vary between 26 and 31 mg NO_3 l^{-1}, which induces a reduction in the gobal

Table V. Variogram analysis

Gauging station	ρ				Sill ratio			
	nug	exp	perio	global	nug	exp	perio	global
Choisy	0·7	0·91	0·99	0·97	1	0·83	0·96	0·94
Ivry	0	0·67	0·85	0·71	1	1·25	0·83	0·92
Suresnes	0·71	0·94	0·99	0·96	0·5	0·88	0·78	0·78
Argenteuil	1	0·8	0·98	0·95	1	1	0·82	0·86
Chatou	0	0·94	1	0·93	1	0·88	0·74	0·76
Bougival	0	0·85	0·99	0·9	1	0·73	0·73	0·74
Sartrouville	0	0·95	0·97	0·92	1	0·67	0·54	0·57
Conflans	0	0·63	0·98	0·83	0·33	0·78	0·92	0·87
Poissy	0	0·91	0·98	0·90	0	0·83	0·96	0·87

ρ: correlation coefficient between measurements and ProSe outputs. Sill ratio: $sill\gamma_{prose}/sill\gamma_{obs}$. *nug*, *exp*, and *perio* stand for the nugget effect, the exponential and the periodical component, respectively.

Copyright © 2010 John Wiley & Sons, Ltd.

sill. Simulated and observed values seem in agreement: Figure 7 indicates that γ_O and γ_S do represent the same process. But, Figure 8 shows that the two variables are poorly correlated (the cross-variogram is lower than the simple ones). This discrepancy between the ProSe values and the observed values might be due to a wrong quantification of the outflow either of the Seine Amont WWTP located in the city of Valenton or of an important CSO located in this river section. The Seine Amont WWTP treats the waste waters from 1·8 M inhabitants and the mean concentration of nitrate in its outflow is 102 mg NO_3 l^{-1}, whereas the discharge of the CSO varies between 0·5 and 6 m^3 s^{-1} and its nitrate concentration is poorly known.

From Ivry to Suresnes. At Suresnes, the variogram pattern changes to $\gamma_S < \gamma_{OS} < \gamma_O$. The discontinuity between Ivry and Suresnes is due to the Marne River, which represents a significant contribution to the Seine discharge after the confluence of the two rivers.

From Suresnes to Sartrouville. From Suresnes to Sartrouville, ProSe does not simulate in a satisfactory way the periodic component of γ_O (sill ratio ω_{perio} ranging between 0·54 and 0·82) even if the correlation coefficients are good (between 0·97 and 1). This is almost the same for the exponential component, except for Argenteuil where the sill ratio equals 1. For this group of sites, the variogram analysis reveals that ProSe reproduces more or less the nitrate fluctuations but reduces the temporal variability. Between Suresnes and Argenteuil, there is almost no difference between the variogram patterns although a major CSO is located in this river section. The CSO seems to be properly characterized (in time, discharge and concentrations) since, in Argenteuil, the three variograms are very similar (Figure 8). There are no significant inputs (WWTP, confluence or CSO) between Argenteuil and Sartrouville, but discrepancies between variogram sills increase from upstream to downstream. Thus, this discrepancy between γ_O and γ_S can be explained by the fact that the physical processes are not modelled properly and/or that the parameter values are not well calibrated. Figure 7 suggests an explanation for the source of this discrepancy. Indeed for Chatou, Bougival and Sartrouville, the simulated concentrations are overestimated from day 150 to the end of the simulation. This can be explained by an overestimation of the nitrification or an underestimation of the denitrification within sediments that affects the nitrate concentrations in the water column due to diffusion at the sediment-water interface. This is confirmed by the fact that temporary inputs such as CSO do have a significant effect on the long-term variability of the nitrate concentrations in the river (Even, 2007a) due to sedimentation processes.

From Sartrouville to Conflans. At Conflans, the experimental variograms are crossing each other. This indicates that the three components of the linear model of co-regionalization interact in a complex way, but the $\gamma_{OS} < \gamma_S$ for the first 4 months (<120 days, Figure 8). Figure 7 indicates that the nitrate concentrations simulated by ProSe are underestimated from the late summer to the end of the year. The global determination coefficient ρ^2 is only 0·69 ($\rho = 0{\cdot}83$ in Table V). The periodic component is consistent between γ_O and γ_S. The main issue is due to the exponential component and the nugget effect: the components corresponding to sub-weekly (nugget effect) and monthly (exponential component) variabilities are not well reproduced by ProSe. In addition, contrary to the other sites, most of the simulated values are underestimated (Figure 7). This might be explained by an overestimation of the denitrification by the model in the Seine River. An overestimation of the denitrification process seems realistic since an important sedimentation prevails in this area and denitrification in this context is difficult to simulate accurately.

From Conflans to Poissy. At Poissy, the periodic component of γ_S is consistent with the observed one with $\rho = 0{\cdot}98$ and a sill ratio of 0·96 (Table V). For the exponential component, the sill ratio is only 0·83, but the determination coefficient ρ^2 is 0·83 ($\rho = 0{\cdot}91$). The main point at Poissy is revealed by the nugget effect (2 (mg NO_3 l^{-1})^2 in Table IV). It is the highest observed nugget effect among those calculated at the measurement sites, whereas it is null when calculated from the ProSe results. The change in the variogram pattern might be due to the confluence of the Seine and the Oise Rivers. The fact that γ_O and γ_S are not equal also results from all modelling approximations previously mentioned.

CONCLUSION

The exploratory geostatistical analysis enables us to point out and to better understand errors in data used as model inputs and errors in data used to compare model outputs with.

Co-kriging made possible the building of a consistent homogeneous dataset of upstream BCs (input data) and of data validation.

After this data processing, the ProSe model was run to simulate water quality in the river. The comparison of the simulated values with the observed ones leads to the conclusion that nitrate are rather well simulated by the model. The statistical single criteria (average values, standard deviation and RMSE) seem to be also good.

But the analysis of simple variograms of observed and simulated nitrate and their cross-variogram reveals a clear mismatch between the simulated values and the observed ones that was not revealed by the other objective functions. It also makes it possible to analyse the model response with regard to measurements in terms of three different time step responses (sub-weekly, monthly and annual). Moreover, as BCs were processed in order to obtain a consistent dataset, mismatches were analysed as inadequate quantification of inputs to the river and an approximated description of the physical processes

Copyright © 2010 John Wiley & Sons, Ltd.

within the river. This analysis results in pointing out (i) model inconsistencies in terms of input data (tributary, CSO, WWTP contributions to the nitrate fluxes in the Seine River) and (ii) wrong descriptions of the physical processes, either conceptual or due to the parameter calibration. It therefore helps to identify more precisely the uncertainty sources due to sub-optimal parameter values and internal model structure, and to locate them in the modelled area.

Finally, this type of analysis should be developped in distributed modelling more widely in order to improve model quality by understanding and characterizing different types of uncertainty sources.

ACKNOWLEDGEMENTS

This research project was granted by the Carnot MINES Institute, and part of the PIREN Seine research program on the Seine Basin. The authors are grateful to SIAAP (Sewage Public Company of the Greater Paris), to VNF (National Organisation for River Navigation, in charge of Surface Water Quality Control) and Veolia Water for the data they supplied and the interesting discussions concerning the Seine River water quality. The authors are also grateful to the reviewers for their attentive reading and their useful comments.

REFERENCES

Ambrose R, Barnwell T, McCutcheon S, Williams J. 1996. Water resources handbook. *Computer Models for Water Quality Analysis*. McGraw-Hill: New York. Chapter 14.

Ambrose RB, Wool TA, Wool JP, Schanz RW. 1988. WASP4, A hydrodynamic and water quality model. *Model Theory, User's Manual Guide and Programmer's Guide*. US Environmental Protection Agency: Athens, GA, USA.

Anderton S, Latron J, Gallart F. 2002a. Sensitivity analysis and multiresponse, multi-criteria evaluation of a physically based distributed model. *Hydrological Processes* **16**: 333–353.

Anderton S, Latron J, White S, Llorens P, Gallart F, Salvany C, O'Connell P. 2002b. Internal evaluation of a physically based distributed model using data from a Mediterranean mountain catchment. *EGS* **6**(1): 67–83.

Arheimer B, Olsson J. 2003. Integration and coupling of hydrological models with water quality models: applications in Europe. Technical Report, Workgroup Report, WMO RA VI (K55·1·02).

Arhonditsis G, Brett M. 2004. Evaluation of the current state of mechanistic aquatic biogeochemical modeling. *Marine Ecology Progress Series* **271**: 13–26.

Bagnold R. 1966. An Approach to the Sediment Transport Problem from General Physics. Physiographic and Hydraulic Studies of Rivers. Technical Report., Geological Survey Professional paper 422-I.

Barnwell T, Brown L, Whittemore R. 1987. QUAL2E - a case study in water quality modelling software. *Systems Analysis in Water Quality Management*. Pergamon Press: New York; 377–387.

Beven K. 1989. Changing ideas in hydrology: the case of physically-based model. *Journal of Hydrology* **105**: 157–172.

Beven K. 1993. Prophecy, reality and uncertainty in distributed hydrological modelling. *Advances in Water Resources* **16**: 41–51.

Beven K. 2006a. A manifesto for the equifinality thesis. *Journal of Hydrology* **320**: 18–36.

Beven K. 2006b. On undermining science? *Hydrological Processes* **20**: 3141–3146.

Billen G, Garnier J, Hanset P. 1994. Modelling phytoplankton development in whole drainage networks: the RIVERSTRAHLER model applied to the Seine river system. *Hydrobiologia* **289**: 119–137.

Billen G, Garnier J, Meybeck M. 1998. Les sels nutritifs : l'ouverture des cycles. *La Seine en son bassin. Fonctionnement écologique d'un système fluvial anthropisé*. Elsevier: Paris, France; 531–535.

Billen G, Garnier J, Rousseau V. 2005. Nutrient fluxes and water quality in the drainage network of the scheldt basin over the last 50 year. *Hydrobiologia* **540**(1–3): 47–67.

Billen G, Servais P. 1989. Modélisation des processus de dégradation bactérienne de la matière organique en milieu aquatique. In *Micro-organismes dans les écosystèmes océaniques*, Bianchi M (ed.) Masson: Paris; 219–245.

Billen G, Servais P, Becquevort S. 1990. Dynamics of bacterioplankton in oligotrophic and eutrophic aquatic environments: bottom-up or top-down control? *Hydrobiologia* **207**(1): 37–42.

Billen G, Garnier J, Ficht A, Cun C. 2001. Ecological modeling of the 50 last years of anthropogenic impact in the seine estuary. *Estuaries* **24**(6): 977–993.

Boudreau BP. 1997. *Diagenetic Models and their Implementation*. Springer: Berlin, Germany.

Brown LC, Barnwell TO. 1987. Enhanced stream water quality models, QUAL2E and QUAL2E UNCAS—Documentation and user's TechReport. US EPA.

Butts M, Payne J, Kristensen M, Madsen H. 2004. An evaluation of the impact of model structure on hydrological modelling uncertainty for streamflow simulation. *Journal of Hydrology* **298**: 242–266.

Casper M, Vohland M. 2008. Validation of a large scale hydrological model with data fields retrieved from reflective and thermal optical remote sensing data—a case study for the upper rhine valley. *Physics and Chemistry of the Earth* **33**: 1061–1067.

Chilès J-P Delfiner P. 1999. *Geostatistics: Modeling Spatial Uncertainty*. Wiley: New-York.

Chilès J-P, Séguret S. Riboud P-M. 2008. Geostatistical analysis of validation data of an air pollution simulator. In Proceedings of the 8th International Geostatistics Congress, Santiago, Chile, vol. 2; 861–870.

Crabtree R, Gent R, Clifforde I. 1994. Controlling pollution from combined sewer overflows: practical experience of applying an integrated approach in the UK. *Genie-Urbain-Genie Rural* **5**: 269–272.

de Fouquet C. 2006. La modélisation géostatistique des milieux anthropisés. Académie de Paris, Université Pierre et Marie Curie.

Ebel B, Loague K. 2006. Physics-based hydrologic-response simulation: seeing through the fog of equifinality. *Hydrological Processes* **20**: 2887–2900.

Even S, Mouchel J-M, Servais P, Flipo N, Poulin M, Blanc S, Chabanel M, Paffoni C. 2007. Modeling the impacts of combined sewer overflows on the river Seine water quality. *Science of the Total Environment* **375**(1–3): 140–151.

Even S, Poulin M, Garnier J, Billen G, Servais P, Chesterikoff A. Coste M. 1998. River ecosystem modelling: application of the PROSE model to the Seine river (France). *Hydrobiologia* **373**: 27–37.

Even S, Poulin M, Mouchel J-M, Seidl M, Servais P. 2004. Modelling oxygen deficits in the Seine river downstream of combined sewer overflows. *Ecological Modelling* **173**: 177–196.

Fischer H., Pusch M. 2001. Comparison of bacterial production in sediments and epiphyton and the pelagic zone of a lowland river. *Freshwater Biology* **46**: 1335–1348.

Flipo N, Even S, Poulin M, Tusseau-Vuillemin M-H, Améziane T, Dauta A. 2004. Biogeochemical modelling at the river scale: Plankton and periphyton dynamics—Grand Morin case study, France. *Ecological Modelling* **176**: 333–347.

Flipo N, Even S, Poulin M, Théry S, Ledoux E. 2007a. Modelling nitrate fluxes at the catchment scale using the integrated tool CAWAQS. *Science of the Total Environment* **375**: 69–79.

Flipo N, Jeannée N, Poulin M, Even S, Ledoux E. 2007b. Assessment of nitrate pollution in the Grand Morin aquifers (France): combined use of geostatistics and physically-based modeling. *Environmental Pollution* **146**(1): 241–256.

Flipo N, Rabouille C, Poulin M, Even S, Tusseau-Vuillemin M, Lalande M. 2007c. Primary production in headwater streams of the Seine basin: the Grand Morin case study. *Science of the Total Environment* **375**: 98–109.

Garnier J, Billen G, Coste M. 1995. Seasonal succession of diatoms and chlorophycae in the drainage network of the river Seine: observations and modelling. *Limnology and Oceanography* **40**(4): 750–765.

Garnier J, Billen G, Hannon E, Fonbonne S, Videnina Y, Soulie . 2002. Modeling transfer and retention of nutrients in the drainage network of the danube river. *Estuarine Coastal And Shelf Science* **54**: 285–308.

Garnier J, Billen G, Hanset P, Testard P, Coste M. 1998. Développement algual et eutrophisation dans le réseau hydrographique de la Seine. In *La Seine en son bassin-Fonctionnement écologique d'un système fluvial*

Copyright © 2010 John Wiley & Sons, Ltd.

anthropisé, Meybeck M, de Marsily G., Fustec E (eds). Elsevier: Paris, France; 593–626.
Garnier J, Billen G, Sanchez N, Leporcq B. 2000. Ecological functioning of the Marne reservoir (upper Seine basin, France). *Regulated Rivers-Research & Management* **16**: 51–71.
Garnier J, Némery J, Billen G, Théry S. 2005. Nutrient dynamics and control of eutrophication in the Marne river system: modelling the role of exchangeable phosphorus. *Journal of Hydrology* **304**: 397–412.
Güntner A, Uhlenbrook S, Seibert J, Leibundgut C. 1999. Multicriterial validation of TOPMODEL in a mountainous catchment. *Hydrological Processes* **13**: 1603–1620.
Ivanov P, Masliev I, Kularathna M, De Marchi C, Somlyody L. 1996. DESERT User's manual. Technical Report. International Institute for Applied Systems Analysis, Austria - Institute for Water and Environmental Problems: Russia.
Lancelot C, Veth C, Mathot S. 1991. Modelling ice-edge phytoplankton bloom in the scotia-weddell sea sector of the southern ocean during spring 1998. *Journal of Marine Systems* **2**: 333–346.
Maldiney M-A. 1994. Caractéristiques physiques des particules en suspension dans un fleuve canalisé, exemple de la Seine. PhD thesis. Ecole Nationale des Ponts et Chaussées.
McCarter L. 1999. The multiple identities of vibrio parahaemolyticus. *Journal of Molecular Microbiology and Biotechnology* **1**(1): 51–57.
Nash J, Sutcliffe J. 1970. River flow forecasting through conceptual models. Part I, a discussion of principles. *Journal of Hydrology* **10**: 282–290.
Polus-Lefebvre E, de Fouquet C, Bernard-Michel C, Flipo N, Poulin M. 2008. Geostatistical model for concentrations or flow rates in streams: some results. In Proceedings of the 8th International Geostatistics Congress, Santiago, Chile, vol. 2; 871–880.
Poulin M. 2006. Réalisation de simulations PROSE - Année de référence 2003. Technical Report. Centre de Géoscieces - Mines ParisTech: Paris, France.
Prosser I, Rustomji P. 2000. Sediment transport capacity relations for overland flow. *Progress in Physical Geography* **24**(2): 179–193.
Quynh L, Billen G, Garnier J, Théry S, Fezard C, Minh C. 2005. Nutrient (N,P) budgets for the Red River basin (Vietnam and China). *Global Biogeochemical Cycles* **19**(2): GB2002.
Refsgaard J. 1997. Parameterisation, calibration and validation of distributed hydrological models. *Journal of Hydrology* **198**: 69–97.
Reichert P. 1994. AQUASIM- a tool for simulation and data analysis of aquatic systems. *Water Science and Technology* **30**(2): 21–31.
Reichert P, Borchardt D, Henze M, Rauch W, Shanahan P, Somlyódy L, Vanrolleghem P. 2001a. River water quality model No.1. Technical Report. IWA: London, UK.
Reichert P, Borchart D, Henze M, Rauch W, Shanahan P, Somlyody L, Vanrolleghem P. 2001b. River water quality model no. 1: II. biochemical process equations. *Water Science and Technology* **43**(5): 11–30.
Sferratore A, Billen G, Garnier J, Théry S. 2005. Modeling nutrient (N,P,Si) budget in the Seine watershed: application of the Riverstrahler model using data from local to global scale resolution. *Global Biogeochemical Cycles* **19**(4): GB4S07.
Streeter H, Phelps EB. 1925. A study of the pollution and natural purification of the Ohio River. Technical Report Public Health Bulletin No. 146. U.S. Public Health Service, Treasury Department: Washington, DC.
Tayfur G. 2002. Applicability of sediment transport capacity models for nonsteady state erosion from steep slopes. *Journal of Hydrologic Engineering* **7**(3): 252–259.
Wells S. 2000. Hydrodynamic and water quality river basin modelling using CE-QUAL version3. In *Development and Application of Computer Technics to Environmental Studies*, Ibarra-Berastegi G, Brebbia C, Zannetti P (eds). WIT Press: Boston, MA.
Wool T, Ambrose R, Martin J, EC. 2001. Water Quality Analysis Simulation Program (WASP) version 6.0 - User's manual. Technical Report. US EPA: Athens, GA, USA.
Yang C. 1996. *Sediment Transport Theory and Practice*. McGraw-Hill: New York.

APPENDIX A: DESCRIPTION OF THE PROSE MODEL

In the following paragraphs, the biogeochemical part of PROSE is summarized. A few parameters are temperature dependent (i.e. they are multiplied by a function of the water temperature expressed in °C, $f(T)$) as follows:

$$f(T) = f(T_{\text{opt}})e^{-(T-T_{\text{opt}})^2/\sigma^2} \tag{7}$$

where T_{opt} is the optimal temperature (maximum of f), and σ is the standard deviation of T time series. In the remaining, those parameters are represented with the symbol^T.

Primary Producers

The conceptual scheme used to model the dynamics of PPs was developed by (Lancelot *et al.*, 1991). It is based on the interpretation of experiments incorporating marked carbon into various cell constituents. PP growth follows a photosynthesis-irradiance law:

$$P(z) = P^T_{\max}(1 - e^{-\alpha I(z)/P^T_{\max}})\ e^{-\beta I(z)/P^T_{\max}} \tag{8}$$

where $P^T_{\max}$ is the maximum photosynthesis production rate ([T^{-1}]), $P(z)$ the actual growth rate at z ([T^{-1}]), $I(z)$ the actual irradiance at z ([μE L^{-2}T^{-1}]), α the slope of the light-limited portion of $P-I$ curve or the photosynthesis capacity ([L^2]), and β the photoinhibition coefficient ([L^2 μE^{-1}]).

The actual irradiance at z follows a Beer-Lambert law:

$$I(z) = I_0 e^{-\eta z} \tag{9}$$

where I_0 is the light intensity at the water surface ([μE L^{-2}T^{-1}]), η is the actual light extinction ([L^{-1}]) depending on suspended matter concentration (SM, [ML^{-3}]):

$$\eta = \eta_{const} + \eta_{\text{SM}} SM \tag{10}$$

with η_{const} the water light extinction coefficient ([L^{-1}]) and η_{SM} the light extinction due to SM ([L^{-1}]).

The maximum rate of growth for primary producers ($\mu_{max,PP}$, [T^{-1}]) is then calculated by integrating $P(z)$ over the water column depth (h, [L^{-1}]):

$$\mu_{max,PP} = \frac{1}{h}\int_0^h P(z)dz \tag{11}$$

The actual growth rate (μ_{PP}, [T^{-1}]) is weighted by nutrient concentrations in the following way:

$$\mu_{PP} = \mu_{max,PP}\frac{N}{N+K_N}\frac{PO_4}{PO_4+K_{PO_4}} \tag{12}$$

where N is the concentration of nitrogen (either ammonium or nitrate) that is consumed by PP ([ML^{-3}]), PO_4^{3-} is orthophosphate concentration ([ML^{-3}]), K_i is the half saturation constant for the i$^{\text{th}}$ species ([ML^{-3}]).

Losses (L in Equation 13, [T^{-1}]) are due to respiration (R_{tot} in Equation 14, [T^{-1}]), mortality (Mort^T_{PP}, [T^{-1}]) and sedimentation:

$$L = R_{tot} + Mort^T_{PP} + \frac{V_{sed,PP}}{h} \tag{13}$$

$$R_{tot} = R^T_M + R_\mu \mu \tag{14}$$

Copyright © 2010 John Wiley & Sons, Ltd.

where R_M^T is the basic respiration rate ([T^{-1}]), R_μ is the respiration rate due to growth (without dimension), and $V_{sed,i}$ the sedimentation velocity of the ith species ([LT^{-1}]).

Finally, the variation of the *PP* concentration ([ML^{-3}]) over a time step *dt* is given by:

$$\frac{dPP}{dt} = \left(\mu_{PP} - R_{tot} - Mort_{PP}^T - \frac{V_{sed,PP}}{h}\right) PP \quad (15)$$

Bacteria

The evolution of organic matter (particulate and dissolved) and heterotrophic bacteria (HB) populations is based on the HSB model (Billen and Servais, 1989). The variation of HB concentration ([ML^{-3}]) is represented by:

$$\frac{dHB}{dt} = \begin{pmatrix} \mu_{max,HB}^T \dfrac{O_2}{K_{O_2} + O_2} \dfrac{DOM}{K_{DOM} + DOM} \\ -\dfrac{V_{sed,HB}}{h} - Mort_{HB}^T \end{pmatrix} HB \quad (16)$$

where *DOM* is the concentration of dissolved organic matter ([ML^{-3}]). If the oxygen concentration is lower than $O_{2,denit}$ (fitted at 1 mgO_2 L^{-1}), then HB use nitrates to oxidize the dissolved organic matter. The O_2 threshold represents the denitrifying process.

The variation of nitrifying bacteria concentration (NB, [ML^{-3}]) is represented by:

$$\frac{d\ NB}{dt} = \begin{pmatrix} \mu_{max,NB}^T \dfrac{O_2}{K_{O_2} + O_2} \dfrac{NH_4}{K_{NH_4} + NH_4} \\ -\dfrac{V_{sed,NB}}{h} - Mort_{NB}^T \end{pmatrix} NB \quad (17)$$

Difference between sediments and water column

All processes presented above occur in the water column. In sediments, PPs do not grow and there is no sedimentation for any species. It is also possible to define different kinetics parameter values in water column and in sediment for bacteria, even heterotrophic or nitrifying, which was not the case in this study. Indeed (Fischer and Pusch, 2001) observed that bacteria are smaller in the pelagic zone than in sediments. (McCarter, 1999) showed that multicellular behaviour and growth is complex in organized communities and that it could differ from those of single cells.

Exchanges between water column and sediments

The exchange flux between the water column and the sediments of the ith dissolved species ($\Phi_{d,i}$, [$ML^{-2}T^{-1}$]) is calculated by considering the diffusion through the limit layer (Boudreau, 1997):

$$\Phi_{d,i} = \beta(C_{s,i} - C_{w,i}) \quad (18)$$

where β is the mass transfer coefficient ([MT^{-1}]), $C_{s,i}$ is the concentration of the ith species in sediments ([ML^{-3}]) and $C_{w,i}$ the concentration of the ith species in the water column ([ML^{-3}]). In ProSe, the formulation $\beta = E_s u_*$ is used where E_s is a fitted coefficient (without dimension and theoretically proportional to the Schmidt number), and $u_* = \sqrt{\frac{\tau}{\rho}}$ is the shear velocity ([LT^{-1}]), where τ is the mean shear stress ([$ML^{-1}T^{-3}$]) and ρ is the water volumic mass ([ML^{-3}]).

At each time step and in each cell of the simulated domain, ProSe calculates a total flux of particulate exchange between the water column and the sediments (Φ_d, [$ML^{-2}T^{-1}$]), which is the sum of an erosion flux (Φ_{ero}, [$ML^{-2}T^{-1}$]) and a sedimentation flux (Φ_{sed}, [$ML^{-2}T^{-1}$]):

$$\Phi_p = \Phi_{ero} + \Phi_{sed} \quad (19)$$

For the ith particulate species, the erosion flux ($\Phi_{ero,i}$, [$ML^{-2}T^{-1}$]) is calculated based on the transport capacity theory Bagnold, 1966; Yang, 1996; Prosser and Rustomji, 2000; Tayfur, 2002). A multi-species approach leads to the formulation (Maldiney, 1994):

$$\Phi_{ero,i} = \chi_i \zeta \frac{1}{\sum_j \chi_j(\rho_j - \rho_w)/\rho_j} \frac{\rho_w g J U}{g} \quad (20)$$

where χ_i is the mass fraction of the ith species in sediments (without dimension), ζ is the percentage of hydraulic power used to maintain all the particles in suspension (without dimension), ρ_j the volumic mass of the jth species ([ML^{-3}]), ρ_w the water volumic mass ([ML^{-3}]), g the acceleration due to gravity ([LT^{-2}]), J the friction slope (without dimension) and U the mean water velocity ([LT^{-1}]).

For the ith particulate species, the sedimentation flux ($\Phi_{sed,i}$, [$ML^{-2}T^{-1}$]) is calculated based on

$$\Phi_{sed,i} = V_{sed,i} C_{w,i} \quad (21)$$

where $V_{sed,i}$ is the sedimentation velocity of the ith species ([LT^{-1}]) and $C_{w,i}$ the concentration of the ith species in the water column ([ML^{-3}]).

APPENDIX B: GEOSTATISTICS

Some basics of geostatistics are developped in the temporal context (1D). First, theoretical and experimental variograms are presented, then geostatistical bivariate models are summarized and finally co-kriging is tackled. For further details, one may consult (Chiles and Delfiner, 1999).

Introduction to geostatistics

A random function (RF) $Z(t)$ is stationary of order two if its expectation (probabilistic average) and its covariance exist and are invariant by translation:

$$E[Z(t)] = m \quad (22)$$

$$Cov(Z(t), Z(t+\tau)) = E[(Z(t) - m)(Z(t+\tau) - m)] = C(|\tau|) \quad (23)$$

Copyright © 2010 John Wiley & Sons, Ltd.

The RF variance is then $Var(Z(t)) = E[(Z(t) - m)^2] = C(0)$.

The correlogram, the correlation coefficient between $Z(t)$ and $Z(t+\tau)$ as a function of the time interval τ, is the ratio between covariance and variance: $r(\tau) = \frac{C(\tau)}{C(0)}$. It can vary between 1 (for $\tau = 0$) and -1. Without any periodic component, it usually decreases and tends to zero when $|\tau|$ tends to the infinite: $r(\tau) \overrightarrow{|\ \tau|} \to \infty 0$.

The theoretical variogram. For RF stationary of order two, the variogram and the covariance provide an equivalent description of the temporal variability; the variogram is written

$$\gamma(\tau) = C(0) - C(\tau). \tag{24}$$

For two main reasons, variograms are prefered to covariances or correlogram in geostatistics:

- it remains defined for 'intrinsic' RF, when the covariance is not stationary or not even defined. This is the case when the variogram does not stabilize around a 'sill', as for instance for the linear variogram. Thus, variogram is more general than the covariance;
- it has interesting properties for inference, i.e. its calculation from data (Chiles and Delfiner, 1999).

The experimental variogram. Practically, data are available only at experimental points; an experimental variogram is then calculated as an average of squared differences:

$$\gamma_{exp}(\tau) = \frac{1}{2.n(\tau)} \sum_{i=1}^{n(\tau)} [(Z(t_i + \tau) - Z(t_i))^2] \tag{25}$$

$n(\tau)$ designating the number of pairs of experimental instants separated from τ.

Since it is calculated on a single realization of the RF, the experimental variogram cannot be considered as a discretization of the 'theoretical' variogram of variable Z (Chiles and Delfiner, 1999). In the monovariate case, experimental simple variogram is then fitted by a function $\gamma(\tau)$ admitting the required mathematical properties. In a similar way, for a bivariate (or multivariate) case, all experimental simple and cross-variograms are fitted by a bivariate (or multivariate) model, in order to ensure consistency between simple and cross-variograms. These fitted (also called modelled) variograms are required for estimation.

Geostatistical bivariate models

Let Z_1 and Z_2 be two stationary RF of order two (StRF), and m_1 and m_2 their expectation, respectively. The couple (Z_1, Z_2) is stationary of order two if the cross-covariance is stationary:

$$Cov(Z_1(t), Z_2(t+\tau)) = E[(Z_1(t) - m_1)(Z_2(t+\tau) - m_2)] = C_{12}(\tau). \tag{26}$$

Two RF are cross-uncorrelated (i.e. they do not have any temporal cross-correlation: $Z_1 \perp Z_2$) if $C_{12}(\tau) = 0$. The cross-variogram between two RF is defined as half the covariance of their increments:

$$\gamma_{12}(\tau) = \frac{1}{2} E[(Z_1(t+\tau) - Z_1(t))(Z_2(t+\tau) - Z_2(t))]. \tag{27}$$

If Z_1 and Z_2 are cross-uncorrelated, then $\gamma(\tau) = 0$; if their cross-covariance is symmetric ($C_{12}(-\tau) = C_{12}(\tau)$), then the cross-variogram is written $\gamma_{12}(\tau) = C_{12}(0) - C_{12}(\tau)$.

The following three bivariate models present an increasing complexity. In the first model ('residual model'), simple relationships exist between two variables Z_1 and Z_2. As this is not necessarily the case experimentally, two other bivariate models are widely used: the 'intrinsic correlation model' and the 'linear model of coregionalization'. The first two models are simplifications of the third one.

The residual model.

$$Z_2(t) = Z_1(t) + R(t) \tag{28}$$

with $Z_1 \perp R$, and γ_1, γ_2, and γ_R, respectively designating the simple variograms of Z_1, Z_2 and R. Simple and cross-variograms of Z_1 and Z_2 are thus written as:

$$\begin{cases} \gamma_2(\tau) = \gamma_1(\tau) + \gamma_R(\tau) \\ \gamma_{12}(\tau) = \gamma_1(\tau) \end{cases} \tag{29}$$

In this model, the cross-variogram between Z_1 and Z_2 and the variogram of Z_1 are equal and lower than the variogram of Z_2.

The intrinsic correlation model. **Definition.** Two RF Z_1 and Z_2 are in intrinsic correlation if their simple and cross-covariances are proportional to each other: $C_{ij}(\tau) = b_{ij} K(\tau)$, where K is a covariance function and $i, j = 1, 2$. To simplify, let's assume that $K(0) = 1$, $b_{11} \neq 0$ and $b_{22} \neq 0$ (a RF with nil variance is a constant).

Properties.

- The cross-covariance of two RF in instrinsic correlation is proportional to one of the simple stationary covariances, and is symmetric. Thus, $C_{12}(-\tau) = C_{12}(\tau)$ and $b_{12} = b_{21}$;
- Simple and cross-variograms also are proportional to each other:

$$\gamma_{ij}(\tau) = b_{ij}\gamma(\tau) \text{ with } \gamma(\tau) = K(0) - K(\tau); \tag{30}$$

- Since $Var(Z_1(t)) = C_{11}(0)$ and $Var(Z_2(t)) = C_{22}(0)$, then

$$b_{11} = Var(Z_1(t)) \text{ and } b_{22} = Var(Z_2(t)). \tag{31}$$

Copyright © 2010 John Wiley & Sons, Ltd.

- If ρ denotes the correlation coefficient between $Z_1(t)$ and $Z_2(t)$ at the same instant t, their cross-covariance is written

$$Cov(Z_1(t), Z_2(t)) = \rho\sqrt{Var(Z_1(t))Var(Z_2(t))}. \quad (32)$$

Thus, $b_{12} = \rho\sqrt{b_{11}b_{22}}$ and $C_{12}(\tau) = C_{12}(0)K(\tau)$.

Model. Let's consider Z_1 and Z_2, two StRF: Equation 24 summarizes the model; demonstrations is given hereafter.

$$\forall i, j : C_{ij}(\tau) = b_{ij}K(\tau) \Leftrightarrow \exists R \mid \begin{cases} Z_1 \perp R \text{ and } C_R(\tau) = C_1(\tau) \\ Z_2(t) = \rho\omega Z_1(t) + \omega\sqrt{1-\rho^2}R(t) \end{cases} \quad (33)$$

Let's assume that $\omega^2 = \frac{b_{22}}{b_{11}}$, with $\omega > 0$: then $Var(Z_2) = \omega^2 b_{11}$.

If $|\rho_{12}| \neq 1$, the two StRF constitute a free system: $Z_2 = \alpha Z_1 + \beta R$, where $R \perp Z_1$. Then $Cov(Z_1(t), Z_2(t)) = \alpha Var(Z_1(t))$ and $\alpha = \rho\sqrt{\frac{b_{22}}{b_{11}}} = \rho\omega$.

One can deduce that $Z_2 = \rho\omega Z_1 + \beta R$; thus the covariance of RF R is stationary and proportional to $K(\tau)$: $\beta^2 C_R(\tau) = C_2(\tau) - \rho^2\omega^2 C_1(\tau)$.

Assuming that $Var(R) = Var(Z_1)$, $\beta^2 C_1(\tau) = \omega^2 C_1(\tau) - \rho^2\omega^2 C_1(\tau)$, thus

$$\beta^2 = \omega^2(1-\rho^2) \text{ and } Z_2 = \rho\omega Z_1 + \omega\sqrt{1-\rho^2}R, \quad (34)$$

with $R \perp Z_1$ and $C_R = C_1$.

Let's notice that if $|\rho_{12}| = 1$, Z_1 and Z_2 are linearly linked: $Z_2 = \omega Z_1 + a$.

$\Leftarrow$ If $Z_2 = \rho\omega Z_1 + \omega\sqrt{1-\rho^2}R$ with $R \perp Z_1$ and $C_R = C_1$, then:

- R is StRF, because its temporal covariance is equal to the one of Z_1;
- the temporal covariance of Z_2 is $C_2 = \rho^2\omega^2 C_1 + \omega^2(1-\rho^2)C_R = \omega^2 C_1$;
- the temporal cross-covariance between Z_1 and Z_2 is written

$$C_{12} = \rho\omega C_1 + \omega\sqrt{1-\rho^2}C_{1R}. \quad (35)$$

But as $R \perp Z_1$, their temporal cross-covariance is null: $C_{1R} = 0$ and thus $C_{12} = \rho\omega C_1$.

In conclusion, given that simple and cross-covariances of Z_1 and Z_2 are proportional to each other, Z_1 and Z_2 are in intrinsic correlation.

The two coefficients ρ and ω have different meanings. The correlation coefficient ρ quantifies the linear link between the variables Z_1 and Z_2 which is maximum if $|\rho| = 1$. The 'sill ratio' ω^2 characterizes the relative amplitude of the fluctuations of both variables. If $\omega = 1$, the simple variograms of both variables are equal.

Note that if $\rho\omega = 1$, then the intrinsic correlation model corresponds to a particular case of the residual model, with γ_R proportional to γ_1.

The linear model of co-regionalization. It generalizes the intrinsic correlation model to several temporal components k with different correlations or different fluctuation amplitudes. In this model, the simple and cross-variograms are linear combinations of the same components $\gamma^k(\tau)$, a component present in the cross-variogram being necessarily present in both simple associated variograms. The model can be seen as a linear combination of several intrinsic correlation models, which can be written as Equation 25. Note that k describes a temporal component and not an exponent.

$$\gamma_{ij}(\tau) = \sum_k^N b_{ij}^k \gamma^k(\tau) \quad (36)$$

Estimation by co-kriging (Chiles and Delfiner, 1999)

Kriging of Z_1 at a given instant t_0 is an optimal linear estimator from experimental values $Z_1(t_\alpha)$; it is written $Z^*(t_0) = \sum_\alpha \lambda_\alpha Z(t_\alpha)$.

Co-kriging consists in estimating the value of variable Z_1 at the instant t_0 thanks to the experimental values of Z_1 and to another variable Z_2 correlated to Z_1 (with for example Z_2 denser sampled than Z_1). The co-kriging of Z_1 by Z_2 at an instant t_0 is written as Equation 26.

$$Z_1^*(t_0) = \sum_{\alpha\in S_1} \lambda_{1\alpha} Z_1(t_{1\alpha}) + \sum_{\alpha\in S_2} \lambda_{2\alpha} Z_2(t_{2\alpha}) \quad (37)$$

The weights $\lambda_{1\alpha}$ and $\lambda_{2\alpha}$ are obtained by minimizing the estimation error variance under non-bias conditions. For unknown and unlinked means of Z_1 and Z_2, this is performed via the linear system presented by Equation 27, which involves simple and cross-variograms $\gamma_{11}(\tau)$, $\gamma_{22}(\tau)$, and $\gamma_{12}(\tau)$.

$$\begin{bmatrix} \gamma_{11}(t_{1\beta} - t_{1\alpha}) & \gamma_{12}(t_{2\alpha} - t_{1\alpha}) & 1 & 0 \\ \gamma_{21}(t_{1\alpha} - t_{2\alpha}) & \gamma_{22}(t_{2\beta} - t_{2\alpha}) & 0 & 1 \\ 1 & 0 & 0 & 0 \\ 0 & 1 & 0 & 0 \end{bmatrix} \times \begin{bmatrix} \lambda_{1\alpha} \\ \lambda_{2\alpha} \\ \mu_1 \\ \mu_2 \end{bmatrix} = \begin{bmatrix} \gamma_{11}(t_0 - t_{1\alpha}) \\ \gamma_{21}(t_0 - t_{2\alpha}) \\ 1 \\ 0 \end{bmatrix} \quad (38)$$

Co-kriging is an exact interpolator, i.e. it goes through the experimental points $Z_1(t_{1\alpha})$: $Z_1^*(t_{1\alpha}) = Z_1(t_{1\alpha})$.

Copyright © 2010 John Wiley & Sons, Ltd.